Spindle assembly requires complete disassembly of spindle remnants from the previous cell cycle

Jeffrey B. Woodruff*, David G. Drubin, and Georjana Barnes
Department of Molecular and Cell Biology, University of California, Berkeley, Berkeley, CA 94720

ABSTRACT **Incomplete mitotic spindle disassembly causes lethality in budding yeast. To determine why spindle disassembly is required for cell viability, we used live-cell microscopy to analyze a double mutant strain containing a conditional mutant and a deletion mutant compromised for the kinesin-8 and anaphase-promoting complex-driven spindle-disassembly pathways (*td-kip3* and *doc1Δ*, respectively). Under nonpermissive conditions, spindles in *td-kip3 doc1Δ* cells could break apart but could not disassemble completely. These cells could exit mitosis and undergo cell division. However, the daughter cells could not assemble functional, bipolar spindles in the ensuing mitosis. During the formation of these dysfunctional spindles, centrosome duplication and separation, as well as recruitment of key midzone-stabilizing proteins all appeared normal, but microtubule polymerization was nevertheless impaired and these spindles often collapsed. Introduction of free tubulin through episomal expression of α- and β-tubulin or introduction of a brief pulse of the microtubule-depolymerizing drug nocodazole allowed spindle assembly in these *td-kip3 doc1Δ* mutants. Therefore we propose that spindle disassembly is essential for regeneration of the intracellular pool of assembly-competent tubulin required for efficient spindle assembly during subsequent mitoses of daughter cells.**

Monitoring Editor
Fred Chang
Columbia University

Received: Aug 16, 2011
Revised: Oct 25, 2011
Accepted: Nov 8, 2011

INTRODUCTION

Eukaryotes have evolved an elegant microtubule-based machine, the mitotic spindle, to partition genetic material accurately during cell division. Although the size and complexity of mitotic spindles differ among species, several fundamental features are conserved. In all cases, mitotic spindles are organized into bipolar arrays composed of two spindle poles from which emanate three types of microtubules: Kinetochore microtubules (kMTs) connect the spindle poles to chromosomes via kinetochores, proteinaceous complexes that assemble on centromeric regions of the chromosome. Interpolar microtubules (ipMTs) extend from opposite poles, overlap, and link together via cross-linking proteins to connect the two spindle poles and provide rigidity to the overall spindle structure. Finally, astral microtubules (aMTs) extend toward the cell cortex and allow the spindle to determine its position relative to the cell boundary and division plane (reviewed in Glotzer, 2009).

The mitotic spindle is an extremely dynamic structure, being assembled de novo, elongated, and summarily disassembled during each round of cell division. Regulation of spindle assembly is described classically by two models (for a comprehensive review, see Walczak and Heald, 2008). In the first model, termed "search and capture," centrosome-nucleated MTs extend and retract until they are captured and stabilized by kinetochores. The second model, termed "self-assembly," posits that chromosomes themselves can nucleate MTs and organize them into bipolar arrays. Specifically, in budding yeast, stabilization and cross-linking of centrosome-generated ipMTs are crucial for bipolar spindle assembly and are driven by the BimC motor proteins Cin8 and Kip1, as well as the Aurora B kinase Ipl1 and the PRC1 homologue Ase1 (Hoyt *et al.*, 1992, 1993; de Gramont *et al.*, 2007; Kotwaliwale *et al.*, 2007).

Late in mitosis, after the spindle is assembled and chromosomes are segregated to opposite poles, the mitotic spindle is quickly disassembled. In budding yeast, the timing of spindle disassembly is regulated in part by a signaling cascade termed the mitotic exit network (MEN). One consequence of MEN signaling is the activation of

This article was published online ahead of print in MBoC in Press (http://www.molbiolcell.org/cgi/doi/10.1091/mbc.E11-08-0701) on November 16, 2011.

*Present address: Max Planck Institute of Molecular Cell Biology and Genetics, Dresden 01307, Germany.

Address correspondence to: G. Barnes (gbarnes@berkeley.edu).

Abbreviations used: aMT, astral microtubule; APC, anaphase-promoting complex; DMSO, dimethyl sulfoxide; GFP, green fluorescent protein; HRP, horseradish peroxidase; HU, hydroxyurea; ipMT, interpolar microtubule; kMT, kinetochore microtubule; MEN, mitotic exit network; RFP, red fluorescent protein; SPB, spindle pole body.

Supplemental Material can be found at:
http://www.molbiolcell.org/content/suppl/2011/11/14/mbc.E11-08-0701.DC1

Cdc14, a phosphatase that opposes Cdk1. Cdc14-mediated dephosphorylation of the anaphase-promoting complex (APC) cofactor Cdh1 allows APC-mediated degradation of spindle-stabilizing proteins, including Cin8 (Hildebrandt and Hoyt, 2001), Ase1 (Juang *et al.*, 1997), and Fin1 (Woodbury and Morgan, 2007). Spindle disassembly is also driven by the Ipl1 kinase, which phosphorylates and inactivates the MT-stabilizing protein Bim1 (EB1 homologue; Buvelot *et al.*, 2003; Zimniak *et al.*, 2009; Woodruff *et al.*, 2010) and phosphorylates and activates the spindle-destabilizing protein She1 (Woodruff *et al.*, 2010). Finally, the kinesin-13 family member Kip3 depolymerizes spindle MTs to facilitate spindle disassembly (Gupta *et al.*, 2006; Varga *et al.*, 2006; Woodruff *et al.*, 2010). Together, these pathways promote disengagement of the spindle halves, arrest of spindle elongation, and initiation of ipMT depolymerization (Woodruff *et al.*, 2010).

In our previous study, we noticed that yeast cells compromised for a single disassembly pathway, which slows but does not completely block spindle disassembly, were viable and experienced growth rates similar to wild-type cells. But yeast cells compromised for two spindle-disassembly pathways, which severely impairs disassembly, were extremely sick or inviable (Woodruff *et al.*, 2010). Interestingly, in severely sick *cdh1Δ kip3Δ* mutants, in which the kinesin-8 and APC^{Cdh1} spindle-disassembly pathways are inactivated, spindles still broke apart due to shearing from cytokinetic ring contraction. The new daughter cells then progressed into G1 but showed impaired viability, indicating that cytokinesis can break the spindle when primary disassembly mechanisms are impaired and allow entry into the next cell cycle. These results suggest the synthetic genetic interaction of *cdh1Δ* and *kip3Δ* is not due to a failure to exit mitosis. Instead, a downstream essential spindle process (e.g., spindle assembly, chromosome segregation, spindle elongation) might be impaired in the cell cycle of the new daughter cells following a round of defective spindle disassembly in the previous cell cycle.

On the basis of those results, we evaluated the importance of spindle disassembly for cell viability. We used live-cell time-lapse microscopy to analyze spindle morphology and dynamics in yeast cells compromised for the kinesin-8 and APC^{Cdh1} spindle-disassembly pathways. Using a conditionally degradable allele of *KIP3* (*td-kip3*) in combination with a *doc1Δ* mutation, we specifically analyzed these mutants after they experienced one round of defective disassembly and then followed the daughter cells as they progressed into the next cell cycle. We found that complete spindle disassembly in the parent cells is essential for assembly of the spindle in the subsequent cell cycle of the daughter cells. Our results indicate that spindle-disassembly factors are not required for spindle pole body (SPB) duplication or disengagement, but rather for maintenance of spindle length, symmetry, and subunit regeneration. Consistent with these findings, exogenous expression of α- and β-tubulin rescued spindle assembly in *td-kip3 doc1Δ* mutants, suggesting the multiple spindle-disassembly pathways serve also to regenerate the tubulin pool necessary for incorporation into the assembling spindle.

RESULTS

Conditional inhibition of the Kip3 disassembly pathway

For this study, we wished to analyze spindle function in daughter cells immediately after the parent cell experienced a round of defective spindle disassembly. Thus we devised a method to conditionally inactivate the Kip3 disassembly pathway by fusing a temperature-sensitive degron tag (Dohmen *et al.*, 1994) to the N-terminus of Kip3 (td-Kip3). Kip3 actively depolymerizes MTs from their plus ends and is necessary for regulation of ipMT and aMT dynamics in vivo (Straight *et al.*, 1998; Gupta *et al.*, 2006; Varga *et al.*, 2006; Woodruff *et al.*, 2010). Consequently, spindles and aMTs are longer in *kip3Δ* cells than in wild-type cells, but the difference in aMT length is more pronounced (Straight *et al.*, 1998; Woodruff *et al.*, 2010). Therefore, to assess the functionality of *td-kip3*, we measured aMT lengths during anaphase in wild-type, *kip3Δ*, and *td-kip3* yeast expressing the MT marker green fluorescent protein (GFP)-Tub1. When incubated at 25°C, aMTs were similar in length in wild-type and *td-kip3* cells (1.40 ± 0.6 µm and 1.35 ± 0.8 µm, respectively), whereas aMTs were longer in *kip3Δ* cells (3.71 ± 2.4 µm; Figure 1, A and B). When incubated at 37°C for 2 h, aMTs became longer in *td-kip3* cells versus wild-type cells (2.50 ± 1.9 µm and 1.46 ± 0.7 µm respectively) but were not quite as long as aMTs observed in *kip3Δ* cells (3.32 ± 2.0 µm; Figure 1, A and B). These results indicate that *td-kip3* behaves as a temperature-sensitive hypomorphic allele.

A

		sample number (n)	Avg. anaphase aMT length(µm)	P-value
25° C	Wild-type	34	1.40 ± 0.6	N.A.
	kip3Δ	28	3.71 ± 2.4	<0.001
	td-kip3	46	1.35 ± 0.8	0.732
37° C	Wild-type	31	1.46 ± 0.7	N.A.
	kip3Δ	38	3.32 ± 2.0	<0.001
	td-kip3	23	2.5 ± 1.9	0.003

B

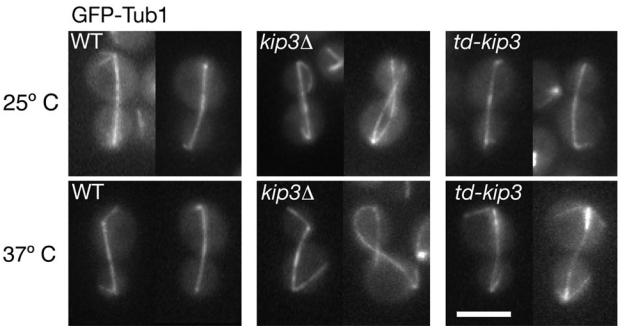

FIGURE 1: *td-kip3* is a conditional hypomorphic allele of *KIP3*. (A) Wild-type, *kip3Δ*, and *td-kip3* cells expressing the MT marker GFP-Tub1 were imaged by live-cell epifluorescence microscopy at 25°C and 37°C. The lengths of aMTs were measured when the cells reached late anaphase (p value calculated using Student's *t* test). (B) Representative images of strains analyzed in (A). Scale bars: 5 µm.

We then examined spindle morphology and dynamics in yeast cells that express *td-kip3* and harbor a null *doc1Δ* mutation. *DOC1* encodes a subunit of the APC required for processive addition of ubiquitin peptides to APC substrates (Hwang and Murray, 1997; Carroll and Morgan, 2002). Similar to *cdh1Δ* cells, *doc1Δ* mutants display hyperstable spindle remnants after mitotic exit, indicating that Doc1 is critical for spindle disassembly (Woodruff *et al.*, 2010). We chose to utilize the *doc1Δ* mutation, because ipMT depolymerization rates indicate that *doc1Δ* cells display a stronger spindle phenotype than do *cdh1Δ* cells (Woodruff *et al.*, 2010). Thus, when incubated at 37°C, *td-kip3 doc1Δ* cells are compromised for the kinesin-8 and APC^{Cdh1} spindle-disassembly pathways.

Defective spindle disassembly inhibits spindle assembly in the subsequent cell cycle

After incubating *td-kip3 doc1Δ* cells at 37°C for 2 h, we followed GFP-Tub1–labeled spindles starting from late anaphase of the parent cell to metaphase of the next cell cycle in the daughter cells.

Spindles broke apart during mitotic exit due to contraction of the cytokinetic ring (Woodruff *et al.*, 2010; unpublished data), and the hyperstable spindle halves eventually disassembled in the daughter cells during G1. In ~8% of cells, we observed spindle remnants that appeared to break off from the spindle half and persist in the daughter cells, sometimes until G2/M (Supplemental Figure S1A and Figure 2A; n = 100). This phenomenon occurred in < 1% of wild-type cells (Figure S1B; n = 210). Thus these results suggest that, while the spindles themselves can be broken apart, the complete depolymerization of spindle MTs is impaired in *td-kip3 doc1Δ* cells.

Surprisingly, although the *td-kip3 doc1Δ* daughter cells continued through the cell cycle and budded, ~41% of the cells could not assemble symmetric bipolar spindles efficiently, and instead assembled spindles that were monopolar, asymmetric, or broken (Figure 2B, panels i–iii). We defined a spindle as "monopolar" if we observed only one spindle pole (indicated by the SPB marker Spc42-eqFP) in the cell; "asymmetric" if we observed two spindle poles connected by MTs, but the GFP-Tub1 fluorescence was >1.5-fold brighter at one pole; and "broken" if we observed two spindle poles that were not connected by spindle MTs. The majority (~59%) of malformed spindles were monopolar. On the other hand, ~99% of wild-type cells similarly analyzed formed proper bipolar spindles (first panel in Figure 2B). These phenotypes suggest that spindle assembly is impaired in *td-kip3 doc1Δ* daughter cells after one round of incomplete spindle disassembly. Furthermore, a direct side-by-side comparison of spindle morphology and GFP-Tub1 fluorescence revealed that bipolar spindles in the *td-kip3 doc1Δ* daughter cells contained, on average, ~2.5-fold less tubulin than did bipolar spindles in wild-type cells (Figure 2C). For this experiment, we used a mix of GFP-Tub1–expressing wild-type and *td-kip3 doc1Δ* cells in which only one of the two strains expressed SPC42-eqFP; this allowed us to distinguish between the strains and make direct comparison of GFP-Tub1 fluorescence under the same conditions. We observed similar results when we separately analyzed wild-type and *td-kip3 doc1Δ* cells both expressing SPC42-eqFP (unpublished data). To assess the functionality of spindles in *td-kip3 doc1Δ* daughter cells, we monitored spindle checkpoint activity by assaying Pds1 (yeast securin) stabilization. Cells were synchronized first with hydroxyurea (HU)-containing medium at 25°C for 2.5 h and then released into α-factor–containing medium at 37°C for 3.5 h. Both cultures were then released and arrested again with HU at 37°C. Finally, cells were released from HU arrest and protein extracts were isolated every 45 min. Over time, Pds1-18Myc levels decreased dramatically in wild-type cells but remained stable in *td-kip3 doc1Δ* cells, indicating that *td-kip3 doc1Δ* daughter cells do not satisfy the spindle checkpoint (Figure 2D). Taken together, these results suggest that *td-kip3 doc1Δ* daughter cells cannot efficiently assemble functional, bipolar spindles after one round of defective spindle disassembly.

The failure to reassemble bipolar spindles was far more pronounced in *td-kip3 doc1Δ* double mutants versus *kip3Δ* or *doc1Δ* single mutants, indicative of a synergistic genetic interaction (Figure S2A). Proper spindle formation is essential for chromosome segregation in subsequent cell cycles and therefore impacts the viability of progeny. Therefore these results strongly suggest the synthetic lethal interaction between *doc1Δ* and *kip3Δ*, as well as between mutants of genes in different spindle-disassembly pathways (Costanzo *et al.*, 2010; Woodruff *et al.*, 2010), results from the inability of the daughter cells to assemble a new mitotic spindle after one round of defective spindle disassembly in the parent cell.

We considered the possibility that Kip3 and Doc1 play heretofore undiscovered roles in spindle assembly, in addition to their roles in driving spindle disassembly. To test this hypothesis, we analyzed spindle morphology in *td-kip3 doc1Δ* cells when td-Kip3 was fully functional during spindle disassembly but then inactivated specifically during spindle assembly in the daughter cells (outlined in Figure 2E).

In budding yeast, spindle assembly begins in late G1 after cells pass START, the point of commitment to the cell cycle (Winey and O'Toole, 2001). Yeast cells can be arrested at START using α-factor (Moore, 1987). Thus, to test for a possible role of Kip3 or Doc1 in spindle assembly, *td-kip3 doc1Δ* cells were arrested in G1 using α-factor for 3 h at 25°C. To inactivate td-Kip3, cells were incubated in α-factor–containing medium at 37°C for an additional 3.5 h. Finally, cells were released into HU-containing medium at 37°C and analyzed microscopically after 3.5 h. We noticed that *td-kip3 doc1Δ* cells exited from G1 into S phase more slowly than wild-type cells at 37°C (Figure S2B). The basis for this phenomenon is currently unclear, although it may be related to microtubule integrity and APC activity, as nocodazole-mediated disruption of microtubules and depletion of Doc1 caused delays in the G1- to S-phase transition (Figure S2C). Thus, to ensure that we evaluated cells in the same cell cycle stage, we optimized the length of the HU arrest so that 90% of both wild-type and *td-kip3 doc1Δ* cells were budded by the time of our analysis (Figure S2B). As an extra precaution, we analyzed spindle morphology only in cells that were shmoo-shaped and budded, as these cells were guaranteed to have passed through our synchronization scheme. Another culture of cells was treated with the same protocol, but kept at 25°C throughout as a control (Figure 2E, blue box). Under this treatment protocol, *td-kip3 doc1Δ* cells formed spindles equally well when incubated at 37°C or 25°C (11.7 ± 2% vs. 10 ± 3% cells with malformed spindles, respectively; Figure 2F, blue box) demonstrating that Kip3 and Doc1 do not serve an essential role in spindle assembly.

Next we analyzed spindle morphology in *td-kip3 doc1Δ* cells when td-Kip3 was inactivated both during spindle disassembly and the subsequent spindle-assembly phase (Figure 2E). *td-kip3 doc1Δ* cells were arrested in G1 using α-factor for 3 h at 25°C. Cells were released into HU-containing medium and incubated at 25°C for 2 h to allow spindle assembly, released, and then transferred to α-factor–containing medium and incubated at 37°C for 3.5 h. Finally, cells were released from α-factor arrest and then arrested in preanaphase with HU and analyzed microscopically. Another culture of cells was treated with the same protocol but kept at 25°C throughout as a control (Figure 2E, red box). Interestingly, under this treatment protocol, the frequency of malformed spindles was 4.8-fold higher in *td-kip3 doc1Δ* cells incubated at 37°C versus 25°C (45.7 ± 4% vs. 9.6 ± 5% cells with malformed spindles, respectively; Figure 2F, red box). Taken together, these results suggest that the malformed spindles seen in *td-kip3 doc1Δ* daughter cells are predominantly a result of defective spindle disassembly in the previous cell cycle of the parent cell.

We also considered the possibility that malformed spindles did not result from defective spindle disassembly, but rather from abnormal gene expression caused by aneuploidy in the division of the *td-kip3 doc1Δ* parent cell. We analyzed chromosome segregation using three different methods: a diploid-mating assay (Sprague, 1991), live-cell microscopy of GFP–labeled chromosome 3 (Straight *et al.*, 1996), and live-cell microscopy of the kinetochore marker Mtw1-red fluorescent protein (RFP). Chromosome missegregation occurred rarely in wild-type and *td-kip3 doc1Δ* cells, although the frequency of missegregation was slightly elevated (~1.5-fold) in *td-kip3 doc1Δ* cells (average of all three experiments; Figure S3). Although we cannot rule out the possibility that a small fraction of malformed spindles seen in *td-kip3 doc1Δ* daughter cells are the result

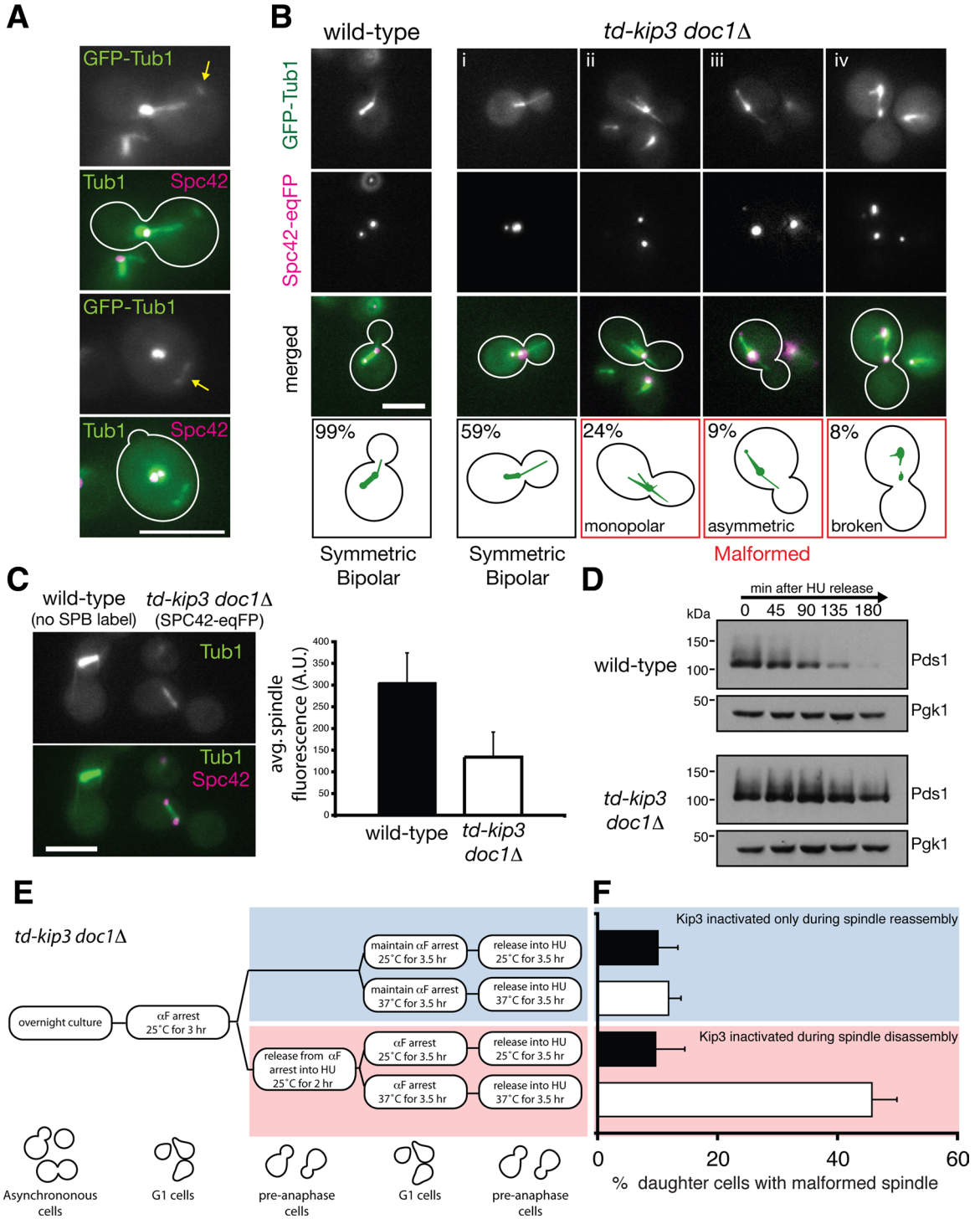

FIGURE 2: Defective spindle disassembly inhibits proper bipolar spindle formation in the subsequent cell cycle. (A) Examples of spindle remnants (yellow arrows) that persisted in *td-kip3 doc1Δ* daughter cells after the mother cell experienced a defective round of spindle disassembly. Spc42-eqFP was visualized as an SPB marker. (B) Spindle morphology in wild-type and *td-kip3 doc1Δ* daughter cells after being incubated at 37°C for 3 h. Spindle morphology classification and frequency are indicated in the boxes in the bottom row (n = 120). Cell borders are outlined in white. (C) Side-by-side comparison of GFP-Tub1 fluorescence in wild-type and *td-kip3 doc1Δ* spindles after one round of spindle disassembly at the nonpermissive temperature (n = 25 for each strain; error bars represent SD). Shown on the left is an image taken from a mixed population of wild-type (no SPB label) and *td-kip3 doc1Δ* cells (Spc42-eqFP–labeled). Scale bars: 5 μm. (D) Following one round of spindle disassembly at the nonpermissive temperature, cells were synchronized with HU and released, and protein extracts were isolated every 45 min. Pds1-18Myc levels were detected by SDS–PAGE followed by immunoblotting. Pgk1 levels were monitored as a loading control. (E) Flowchart describing the experimental procedure. (F) More malformed spindles were seen in *td-kip3 doc1Δ* cells when td-Kip3 was inactivated during spindle disassembly than when td-Kip3 was inactivated during just spindle assembly (n = 3 experiments, each analyzing 30 cells; errors bars represent SD).

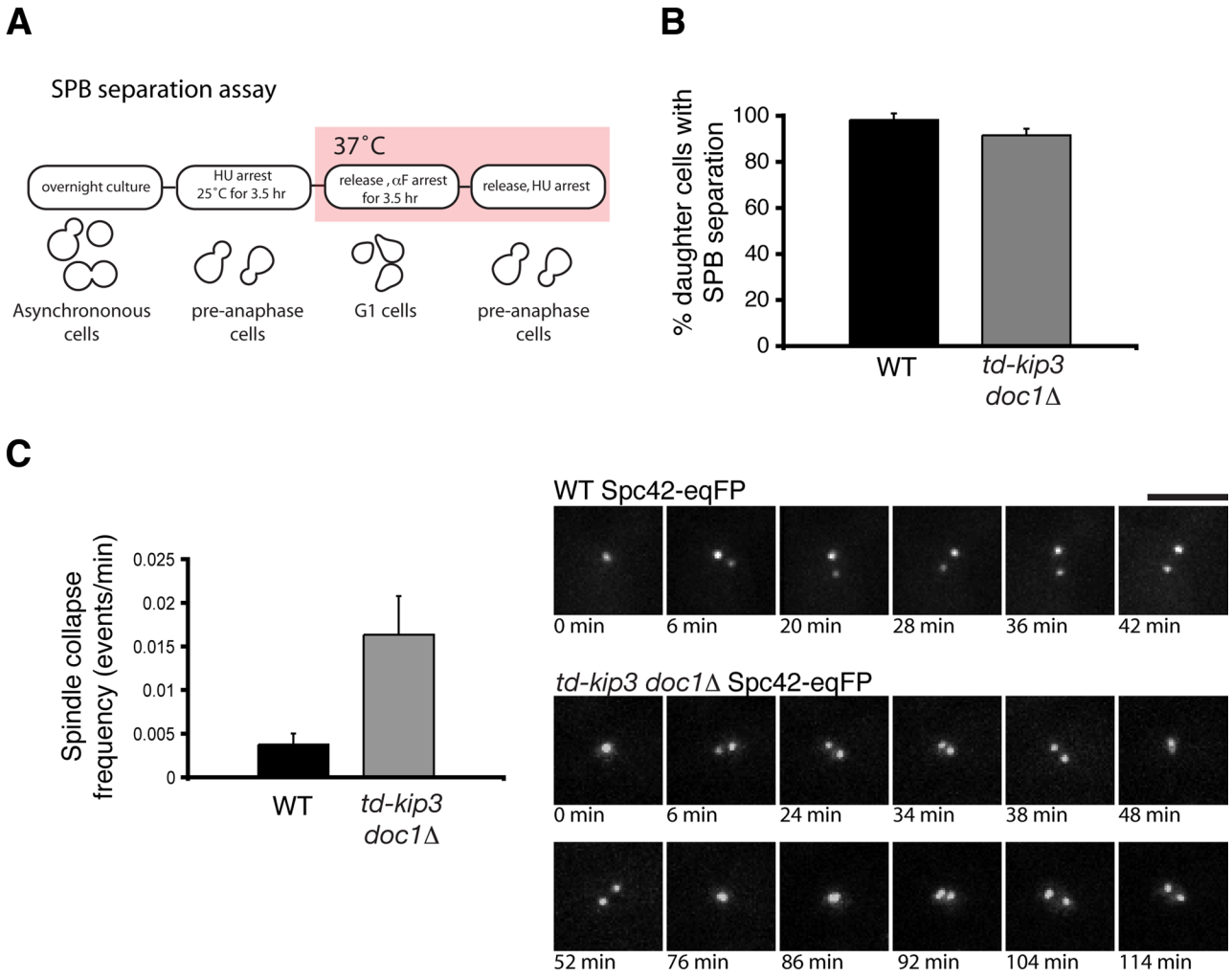

FIGURE 3: SPB separation is perturbed in *td-kip3 doc1Δ* cells. (A) Flowchart describing the experimental procedure. (B) Cells expressing the SPB marker Spc42-eqFP were imaged every 2 min after release from α-factor arrest. After a daughter cell budded, it was followed for 60 min (n = 3 experiments, each analyzing 20 cells; errors bars represent SD). (C) Time-lapse images of SPB separation in wild-type and *td-kip3 doc1Δ* cells expressing Spc42-eqFP after release from α-factor arrest. A spindle collapse event was recorded if separated SPBs came back together to form a monopole (e.g., 76 min, *td-kip3 doc1Δ* cell). Scale bar: 5 μm.

of aneuploidy, the fact that the frequency of malformed spindles is 40-fold higher in *td-kip3 doc1Δ* cells than in wild-type cells strongly argues that gene misexpression due to aneuploidy is not the primary cause of malformed spindles seen in *td-kip3 doc1Δ* mutants.

Monopolar spindles in *td-kip3 doc1Δ* mutants result from spindle collapse, not defective SPB duplication

We set out to address why malformed spindles form in daughter cells after incomplete spindle disassembly in the parent cell. First, we considered the possibility that ipMTs and kMTs still attached to the SPB may remain after incomplete spindle disassembly and interfere with SPB duplication or separation. Certainly, the monopolar spindles observed in *td-kip3 doc1Δ* cells (Figure 2B) were reminiscent of preanaphase spindles seen in *spc42-10* mutant cells, which are defective for SPB duplication (Donaldson and Kilmartin, 1996). However, the fact that we observed mostly bipolar spindles in *td-kip3 doc1Δ* cells (76%; Figure 2B) argues against this point. Still, we tested the hypothesis that SPB duplication failure contributes to the formation of monopolar spindles in *td-kip3 doc1Δ* cells. As outlined in Figure 3A, wild-type and *td-kip3 doc1Δ* cells expressing the spindle pole marker Spc42-eqFP were synchronized in HU-containing medium at 25°C for 3.5 h and then released into α-factor–containing medium at 37°C for 3.5 h. Both cultures were then released into HU-containing medium at 37°C, and SPB duplication was monitored by live-cell, time-lapse microscopy. Sixty minutes after the cells budded, SPB duplication and initial separation occurred in 98% of wild-type cells and 95% of *td-kip3 doc1Δ* cells (Figure 3B). These data suggest SPB duplication failure is not the primary cause of monopolar spindles seen in *td-kip3 doc1Δ* cells.

Combinatorial disruption of Cin8, Kip1, and Ase1—midzone proteins crucial for spindle assembly—prevents SPB separation without affecting SPB duplication (Hoyt *et al.*, 1992, 1993; Roof *et al.*, 1992; Kotwaliwale *et al.*, 2007). Thus we considered the possibility that the monopolar spindles seen in *td-kip3 doc1Δ* cells were caused by a defect in SPB separation. We performed the same experiment as in Figure 3A but measured the distance between separating Spc42-eqFP–labeled SPBs every 2 min. The distance between SPBs in wild-type cells increased and eventually stabilized ~10 min after initial SPB separation, and spindles collapsed only rarely (0.0038 events/min). Strikingly, spindles collapsed more frequently in *td-kip3 doc1Δ* cells (0.0164 events/min; Figure 3C). These results indicate that spindle collapse, rather than defective SPB duplication,

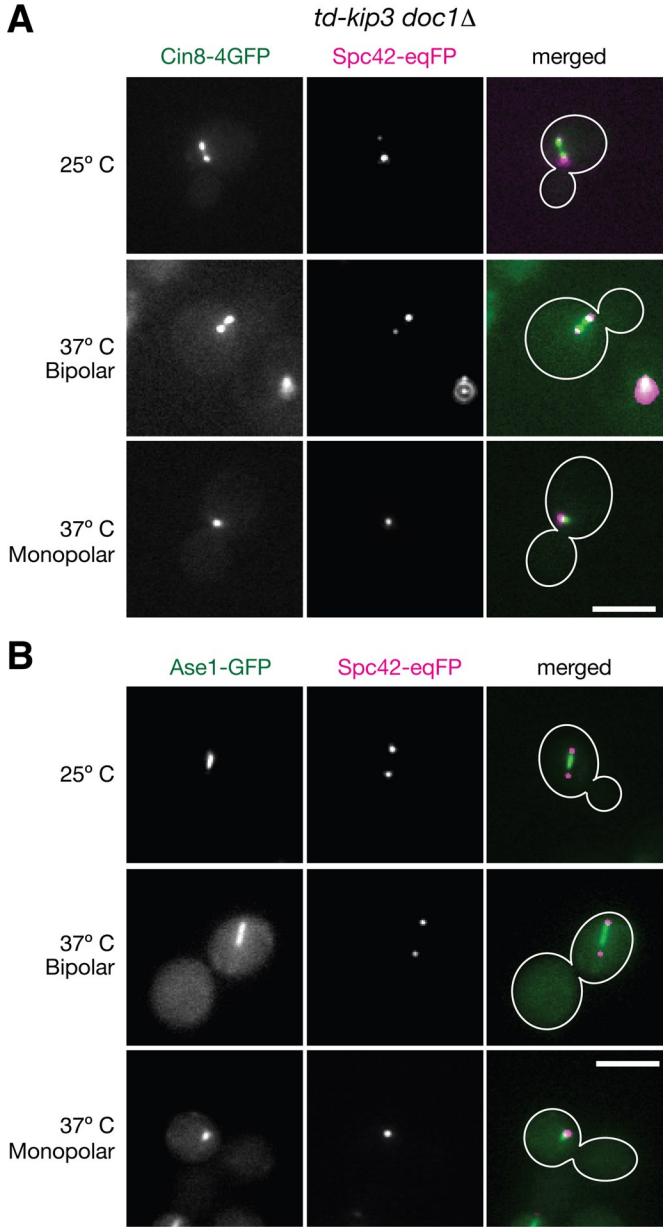

FIGURE 4: Ase1 and Cin8 are recruited to malformed spindles in *td-kip3 doc1Δ* cells. (A) Colocalization of Cin8-4GFP and Spc42-eqFP in *td-kip3 doc1Δ*cells at 25°C and 37°C. Cin8-4GFP appeared on both bipolar and monopolar spindles at the restrictive temperature. (B) Colocalization of Ase1-GFP and Spc42-eqFP in *td-kip3 doc1Δ*cells at 25°C and 37°C. Ase1-GFP appeared on both bipolar and monopolar spindles at the restrictive temperature. Scale bars: 5 μm.

contributes to the formation of monopolar and short spindles seen in *td-kip3 doc1Δ* mutant daughter cells.

We then considered the possibility that SPB separation is defective during spindle assembly in *td-kip3 doc1Δ* daughter cells due to inefficient recruitment of spindle midzone-stabilizing proteins. We analyzed Cin8 and Ase1 recruitment to the spindle by colocalizing Cin8-4GFP and Ase1-GFP with the SPB marker Spc42-eqFP in *td-kip3 doc1Δ* cells arrested in G2/M. In wild-type, preanaphase cells, Cin8 predominantly localizes proximal to SPBs and less prominently to the midzone (Gardner *et al.*, 2008), while Ase1 strongly localizes to the midzone (Khmelinskii *et al.*, 2007). We observed a similar localization for Cin8-4GFP and Ase1-GFP in *td-kip3 doc1Δ* cells incubated for 3 h at either the restrictive or nonrestrictive temperature (Figure 4, A and B). Thus the SPB separation defect observed in *td-kip3 doc1Δ* cells is not due to a failure to recruit Cin8 and Ase1.

Expression of excess free α- and β-tubulin dimers rescues spindle assembly in *td-kip3 doc1Δ* mutants

Spindle assembly not only requires the recruitment of midzone proteins to cross-link antiparallel ipMTs, but also requires MT growth. In budding yeast and metazoans, spindle MTs are highly dynamic when the spindle is assembled (McNally 1996; Nakajima *et al.*, 2011; for a review, see Glotzer, 2009), demanding that a balance be struck between polymerization and depolymerization for elongation and then stabilization of MTs within the spindle. If MT polymerization is reduced or depolymerization is increased, the balance is tipped, and the spindle collapses (Severin *et al.*, 2001; Goshima *et al.*, 2005; Srayko *et al.*, 2005). It is unlikely that MT depolymerization is elevated in *td-kip3 doc1Δ* cells at the nonpermissive temperature, especially since a key depolymerizing factor, Kip3, is absent. Instead, MT polymerization might be inhibited during spindle assembly in *td-kip3 doc1Δ* daughter cells due to the inability to disassemble spindle remnants and regenerate assembly-competent tubulin subunits. This hypothesis is supported by our observation that spindles in *td-kip3 doc1Δ* daughter cells contain less tubulin than do spindles in wild-type cells (Figure 2C).

The growth rate of MTs depends on the concentration of free tubulin dimers (Desai and Mitchison, 1997). Mutations in three genes required for tubulin folding and synthesis, *PAC10*, *PLP1*, and *YAP4*, reduce tubulin levels by 80% and consequently reduce spindle length in anaphase (Lacefield *et al.*, 2006). We analyzed spindle morphology prior to anaphase in *pac10Δ plp1Δ yap4Δ* triple mutants and observed short bipolar, asymmetric bipolar, and monopolar spindles similar to those seen in *td-kip3 doc1Δ* mutants (Figure 5A). This result supports the hypothesis that MT polymerization is impaired during spindle assembly in *td-kip3 doc1Δ* cells after one round of defective spindle disassembly. Tubulin levels are unaffected in *td-kip3 doc1Δ* cells (unpublished data). Thus it is possible that a significant fraction of nuclear tubulin exists in oligomeric states or assembly-incompetent states after incomplete spindle disassembly, resulting in reduced incorporation of tubulin into growing MTs in the daughter cells. If so, we reasoned that providing extra free tubulin dimers might rescue spindle assembly in *td-kip3 doc1Δ* daughter cells.

We transformed *td-kip3 doc1Δ* cells with a 2-μ plasmid containing *TUB1* and *TUB2* (encoding α- and β-tubulin) under the control of a bidirectional galactose-inducible promoter (Burke *et al.*, 1989). *td-kip3 doc1Δ* cells were arrested in G2/M at 25°C, released, and then arrested in G1 at 37°C to inactivate td-Kip3 during spindle disassembly. Throughout this time, cells were incubated in medium containing 1.8% raffinose and 0.2% glucose to silence expression of the episomal *TUB1* and *TUB2* genes. Finally, cells were released from G1 arrest and one-half were transferred to medium containing 1.8% raffinose and 1% galactose to induce episomal *TUB1* and *TUB2* expression (Figure 5B, red box), while the other one-half remained in the raffinose/glucose medium. Another culture of cells was treated using the same protocol, but kept at 25°C throughout as a control (Figure 5B, blue box). Strikingly, at 37°C, episomal tubulin expression dramatically reduced the prevalence of malformed spindles in daughter cells: 17.3 ± 5.8% versus 46.7 ± 1.2% of cells displayed a malformed spindle when incubated in galactose versus glucose, respectively (Figure 5B, red box).

Next we used time-lapse microscopy to monitor rescue of malformed spindles after expression of episomal tubulin. We treated

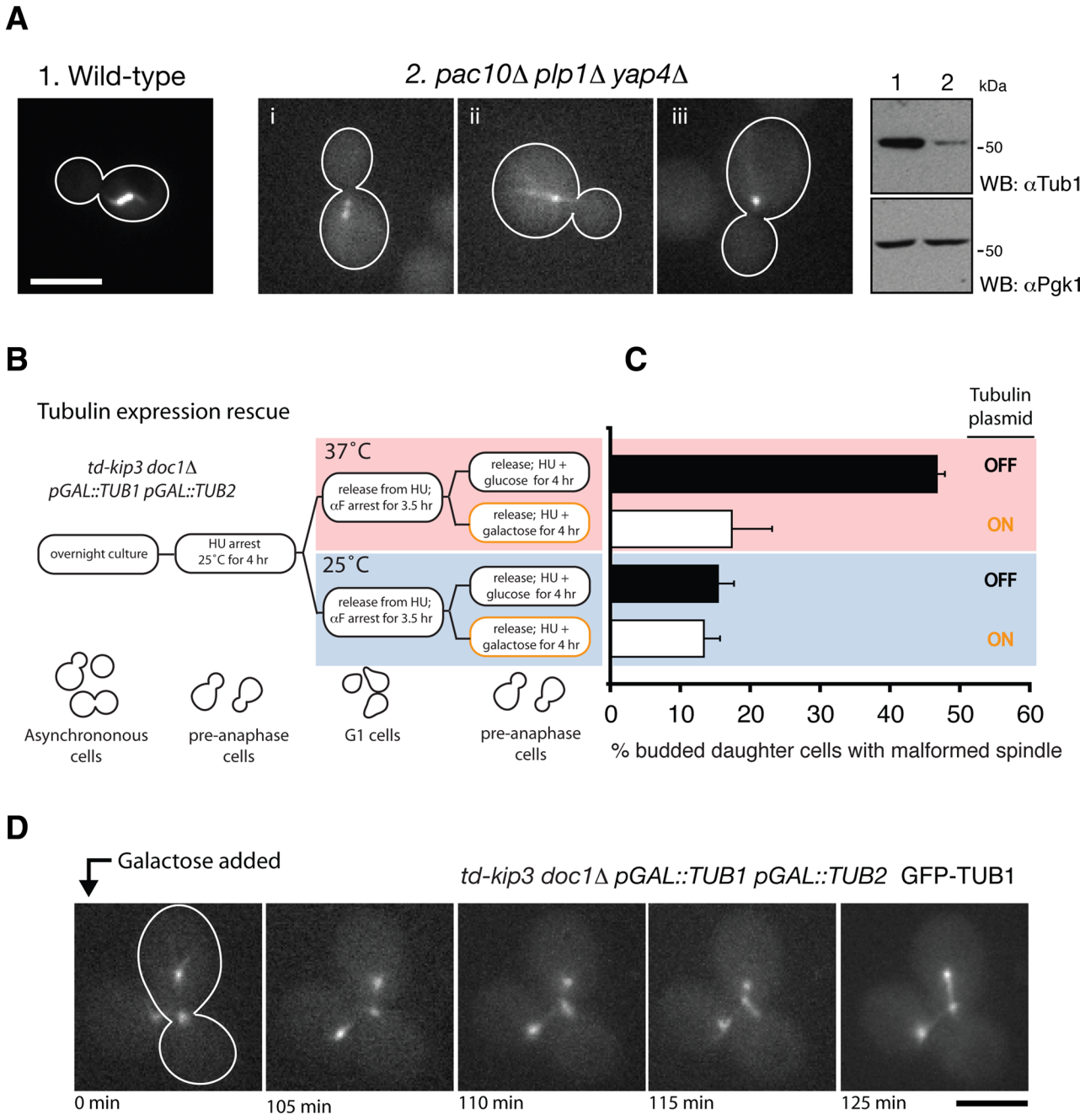

FIGURE 5: Expression of excess free α- and β-tubulin dimers rescues spindle assembly in *td-kip3 doc1Δ* mutants. (A) Epifluorescence images showing examples of spindles in G2/M-arrested wild-type and *pac10Δ plp1Δ yap4Δ* cells expressing the MT marker GFP-Tub1. *pac10Δ plp1Δ yap4Δ* cells display normal bipolar spindles (i), but also asymmetric bipolar (ii), and monopolar (iii) spindles. On the right are immunoblots showing that tubulin levels are reduced in *pac10Δ plp1Δ yap4Δ* triple mutants (lane 2) compared with wild-type cells (lane 1). (B) Flowchart describing the experimental procedure. Cells were examined after the last step by epifluorescence microscopy, and the frequency of malformed spindles for each condition is shown in the graph in (C; n = 3 experiments, each analyzing >50 cells for each condition; error bars represent SD). (D) Time-lapse images of a malformed spindle eventually forming a proper bipolar spindle after 1% galactose was added to induce episomal expression of *TUB1* and *TUB2*. In (A and D), cells are outlined in white. Scale bars: 5 μm.

td-kip3 doc1Δ cells according to the 37°C protocol described above (Figure 5B, red box), except that episomal *TUB1* and *TUB2* expression was induced only after the daughter cells developed malformed spindles in G2/M. Shown in Figure 5D is an example of a broken spindle that eventually formed a proper bipolar spindle after galactose was added to elevate levels of tubulin subunits. These results demonstrate that a supply of free tubulin dimers can rescue spindle assembly in *td-kip3 doc1Δ* daughter cells, supporting the hypothesis that incomplete spindle disassembly prevents MT polymerization during spindle assembly in the subsequent cell cycle.

A pulse of nocodazole rescues spindle assembly in *td-kip3 doc1Δ* mutants

At this point, our results suggested that incomplete disassembly of leftover "parent" spindle MTs impairs regeneration of assembly-competent tubulin needed for proper spindle assembly in the next

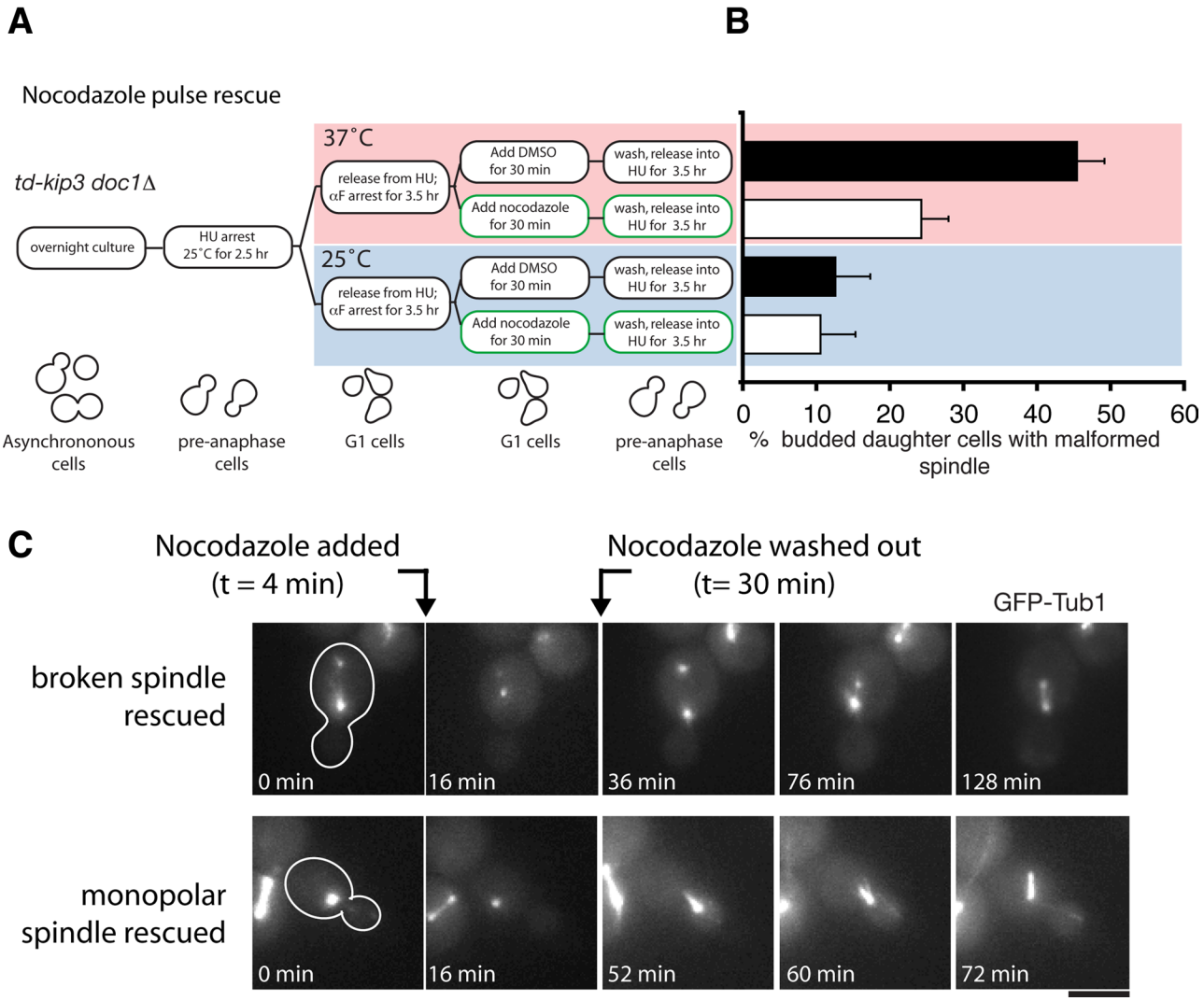

FIGURE 6: Depolymerizing MTs with nocodazole rescues spindle assembly in *td-kip3 doc1Δ* cells. (A) Flowchart describing the experimental procedure. (B) Fewer malformed spindles were seen in *td-kip3 doc1Δ* cells after a 30-min pulse of nocodazole vs. DMSO (n = 3 experiments, each analyzing >50 cells; errors bars represent SD). (C) Time-lapse epifluorescence images of *td-kip3 doc1Δ* cells expressing GFP-Tub1 incubated at 37°C. Cells were treated following the 37°C protocol used in (A), except that nocodazole was not added until after cells were arrested with HU and displayed malformed spindles. Scale bar: 5 μm.

cell cycle of the daughter cells. If this conclusion was correct, we reasoned that providing a pulse of the MT-destabilizing drug nocodazole should depolymerize any leftover spindle remnants and permit proper spindle assembly in *td-kip3 doc1Δ* cells. To perform this experiment, we arrested *td-kip3 doc1Δ* cells in preanaphase using HU at 25°C, released them, and then arrested one-half the culture in G1 using α-factor at 37°C. Daughter cells were then either treated with 5 μM nocodazole or an equal volume of dimethyl sulfoxide (DMSO) for 30 min. Finally, cells were released from the α-factor arrest and spindle formation was analyzed microscopically 3.5 h later (Figure 6A, red box). The other half of the culture of cells was treated using the same protocol but was kept at 25°C throughout as a control (Figure 6A, blue box). The prevalence of malformed spindles was reduced approximately twofold when the nocodazole pulse was applied versus the DMSO pulse for the cells incubated at 37°C (24.2 ± 4% vs. 45.7 ± 4% of cells, respectively; Figure 6B).

Next we used time-lapse microscopy to monitor the process of nocodazole-mediated rescue of malformed spindles. We treated GFP-Tub1–expressing *td-kip3 doc1Δ* cells according to the 37°C protocol used in Figure 6A, except that cells were treated with nocodazole only after they developed malformed spindles in G2/metaphase. Shown in Figure 6C are two examples in which a broken spindle and a monopolar spindle eventually formed bipolar spindles after a 30-min nocodazole pulse. These results show that nocodazole treatment in the daughter cells can allow malformed spindles to "reset" and form proper bipolar spindles.

DISCUSSION

In budding yeast, spindle disassembly is achieved by arrest of spindle elongation, ipMT depolymerization, and disengagement of spindle halves; these subprocesses are largely governed by the Aurora B kinase, kinesin-8, and the APC. This study reveals, surprisingly, that these subprocesses are not essential for spindle breakdown, mitotic exit, and cell division, but rather for spindle assembly in the subsequent cell cycle of the daughter cells. In this paper, we propose that complete spindle disassembly is required to regenerate the pool of

tubulin that is to be incorporated into growing MTs to permit efficient spindle assembly in daughter cells.

Previously we showed that cytokinetic ring contraction can break the spindle and that cells exit mitosis and continue with cell division when the normal mechanisms of spindle disassembly are impaired (Woodruff *et al.*, 2010). However, in the subsequent cell cycle of the daughter cells, the spindle assembles poorly and often collapses or falls apart under these conditions. Four observations suggest these spindles are not completely dysfunctional, but simply lack the necessary pool of assembly-competent tubulin to sustain spindle MT growth. First, the total amount of tubulin incorporated into spindles was ~2.5-fold lower in *td-kip3 doc1Δ* cells as compared with wild-type cells. In addition, we found that aMTs were ~1.8-fold shorter in *td-kip3 doc1Δ* cells versus wild-type cells (Figure S4), suggesting the overall pool of assembly-competent tubulin had been reduced after a round of defective spindle disassembly. Second, during the assembly of these spindles, duplication and initial separation of the spindle MT-nucleating centers, the SPBs, proceeded normally, suggesting SPB biogenesis was not affected. Third, spindles in *td-kip3 doc1Δ* cells recruited key midzone-stabilizing proteins (e.g., Cin8, Ase1). Fourth, malformed spindles displayed the capacity to form stable bipolar structures if provided with free tubulin dimers expressed exogenously from a plasmid source. In light of these observations, the fact that a nocodazole pulse rescues spindle assembly in *td-kip3 doc1Δ* daughter cells following dysfunctional spindle disassembly suggests MTs are not being efficiently depolymerized to generate assembly-competent tubulin dimers, or any assembly-competent oligomeric complex of tubulin, when spindle-disassembly mechanisms are inhibited. The appearance of small, persistent spindle remnants after a defective round of spindle disassembly supports this conclusion. Although the frequency of spindle remnants (8% of cells) did not match the frequency of malformed spindles (40% of cells), a substantial population of small spindle remnants may have escaped our detection due to resolution limitations of light microscopy. However, the fact that the nocodazole-pulse and ectopic tubulin expression experiments did not completely reduce the frequency of malformed spindles to wild-type levels means we cannot conclude that the availability of free tubulin is the sole solution to the problem. There may be other mechanism(s) we have yet to discover, such as improper modification of the pool of free tubulin to make it assembly competent, for example. Moreover, we cannot exclude the possibility that a minority of the spindle defects seen in *td-kip3 doc1Δ* cells resulted from problems unrelated to defective spindle disassembly. Considering that *td-kip3 doc1Δ* cells incubated at the permissive temperature displayed a low frequency of malformed spindles (~9%) and chromosome missegregation (1.5-fold higher than wild-type), it is possible that misexpression of genes vital for spindle assembly may have contributed to the malformed spindle phenotype.

In addition to addressing the importance of spindle disassembly for cell proliferation, our work touches on whether multimeric tubulin assemblies or only tubulin dimers can incorporate into the growing MT polymer. Both in vitro and in vivo studies suggest that actin filaments can grow by incorporating both actin monomers and oligomers (Kawamura and Maruyama, 1970; Murphy *et al.*, 1988; Okreglak and Drubin, 2010). However, it is unclear whether microtubules share this property. It has been demonstrated in vitro that tubulin oligomers can nucleate MTs (Caudron *et al.*, 2002), but whether these oligomers can incorporate into a growing MT sheet remains to be seen. Whether tubulin oligomers per se influence MT nucleation or dynamics in vivo is also unclear. Our work suggests that, in vivo, growth of spindle MTs is sensitive to the oligomeric state of tubulin. It is possible that spindle MTs favor incorporation of tubulin dimers, rather than more complex multimeric assemblies. This proposal seems logical when considering that the growing end of the MT is a curved sheet that eventually zips up to generate a tube (Simon and Salmon, 1990; Chretien *et al.*, 1995). This three-dimensional architecture might favor incorporation of smaller tubulin assemblies (e.g., dimers) and restrict incorporation of higher-order tubulin assemblies that, most likely, do not match the geometry of the growing sheet.

In all eukaryotes, spindle assembly depends on many MT-stabilizing proteins and the availability of assembly-competent tubulin to permit MT polymerization (Goshima *et al.*, 2005; Srayko *et al.*, 2005). Similar to what we and others (Lacefield *et al.*, 2006) have observed for budding yeast, RNA interference–mediated knockdown of the tubulin chaperone prefoldin (PFD-3) decreased α-tubulin levels in the *Caenorhabditis elegans* embryo, resulting in decreased MT polymerization and short metaphase spindles (Lundin *et al.*, 2008). In the future, it will be important to test whether spindle disassembly serves an essential role in tubulin dimer regeneration and/or spindle assembly in *C. elegans* and other metazoans.

MATERIALS AND METHODS

Yeast strains

The yeast strains used in this study are derivatives of S288C and are listed in Supplemental Table S1. Unless denoted otherwise, cells were grown in minimal medium lacking tryptophan or yeast–peptone medium supplemented with 2% glucose. Cells harboring plasmid pDB68 were grown in minimal medium lacking leucine. *td-kip3* was created by cloning a 399-base pair 5′ fragment of *KIP3* into the *Hin*dIII and *Xho*I sites of pPW66R (Dohmen *et al.*, 1994). The resulting plasmid was then cut with *Sna*BI and integrated into the endogenous *KIP3* locus of a wild-type diploid strain. This strain was then sporulated and haploid *kip3Δ::URA3::td-kip3* strains were obtained. The Spc42-eqFP strain was a generous gift from E. Schiebel (ZMBH, Heidelberg, Germany), the *pac10Δ plp1Δ yap4Δ* strain was a gift from S. Lacefield (University of Indiana, Bloomington, IN), and the *pGAL::TUB1 pGAL::TUB2* plasmid (pDB68) was a gift from D. Burke (University of Virginia, Charlottesville, VA).

During our experiments, we noticed that *td-kip3 doc1Δ* cells quickly collected suppressor mutations that rescued the malformed spindle phenotype. Thus, when we performed any experiment involving *td-kip3 doc1Δ* cells, we always struck out the strain(s) from our frozen stock onto yeast–peptone–dextrose or synthetic defined–Leu agar plates, then picked the small colonies and grew them up in liquid medium.

Fluorescence microscopy

Live-cell microscopy at room temperature was performed using an Olympus IX-71 microscope, 100×, numerical aperture 1.4 objective and an Orca-ER camera (Hamamatsu, Hamamatsu City, Japan). All microscopy at 37°C was performed using an Olympus IX-81 microscope equipped with a temperature-controlled enclosure (Precision Control, Fall City, WA), 100×, numerical aperture 1.4 objective, and an Orca-ER camera (Hamamatsu). Two-color images were obtained by sequential switching between RFP and GFP filter sets. For time-lapse microscopy of SPB separation, images were collected every 2 min with 300-ms exposures. For time-lapse microscopy of spindle formation, images were collected every 5 min with 350-ms exposures. Each image represents a maximum intensity projection from a Z-stack containing six planes 0.2 μm apart. When analyzing spindle collapse, we carefully analyzed each plane in the Z-stack to

verify that monopolar spindles were not actually bipolar spindles positioned perpendicular to the slide. All image processing was performed using MetaMorph (Molecular Devices, Sunnyvale, CA).

Immunoblotting

To detect α-tubulin, the membrane was probed with 1:500 anti–TUB1 (Y/OL134; Accurate Chemical and Scientific Corporation, Westbury, NY) and 1:10,000 anti–rat horseradish peroxidase (HRP)-conjugated antibody (GE Healthcare, Waukesha, WI). To detect Pds1-18Myc, the membrane was probed with 1:500 mouse anti-Myc (9E10, our laboratory) and 1:10,000 anti–mouse HRP-conjugated antibody (GE Healthcare). To detect Pgk1, membrane was probed with 1:10,000 anti-Pgk1 (Molecular Probes, Invitrogen, Carlsbad, CA) and 1:10,000 anti–mouse HRP-conjugated antibody (GE Healthcare).

ACKNOWLEDGMENTS

We thank Elmar Schiebel, Soni Lacefield, and Dan Burke for strains. We also thank Rebecca Heald, Yutian Peng, Anthony Cormier, and Nate Krefman for helpful discussions. This work was supported by National Institutes of Health grant GM-47842 to G.B. and a National Science Foundation Graduate Research Fellowship and a Genentech Research Fellowship to J.B.W.

REFERENCES

Burke D, Gasdaska P, Hartwell L (1989). Dominant effects of tubulin overexpression in Saccharomyces cerevisiae. Mol Cell Biol 9, 1049–1059.

Buvelot S, Tatsutani SY, Vermaak D, Biggins S (2003). The budding yeast Ipl1/Aurora protein kinase regulates mitotic spindle disassembly. J Cell Biol 160, 329–339.

Carroll CW, Morgan DO (2002). The Doc1 subunit is a processivity factor for the anaphase-promoting complex. Nat Cell Biol 4, 880–887.

Caudron N, Arnal I, Buhler E, Job D, Valiron O (2002). Microtubule nucleation from stable tubulin oligomers. J Biol Chem 277, 50973–50979.

Chretien D, Fuller SD, Karsenti E (1995). Structure of growing microtubule ends: two-dimensional sheets close into tubes at variable rates. J Cell Biol 129, 1311–1328.

Costanzo M *et al.* (2010). The genetic landscape of a cell. Science 327, 425–431.

de Gramont A, Barbour L, Ross KE, Cohen-Fix O (2007). The spindle midzone microtubule-associated proteins Ase1p and Cin8p affect the number and orientation of astral microtubules in Saccharomyces cerevisiae. Cell Cycle 6, 1231–1241.

Desai A, Mitchison, TJ (1997). Microtubule polymerization dynamics. Annu Rev Cell Dev Biol 3, 83–117.

Dohmen RJ, Wu P, Varshavsky A (1994). Heat-inducible degron: a method for constructing temperature-sensitive mutants. Science 263, 1273–1276.

Donaldson AD, Kilmartin JV (1996). Spc42p: a phosphorylated component of the *S. cerevisiae* spindle pole body (SPB) with an essential function during SPB duplication. J Cell Biol 132, 887–901.

Gardner MK *et al.* (2008). Chromosome congression by Kinesin-5 motor-mediated disassembly of longer kinetochore microtubules. Cell 135, 894–906.

Glotzer M (2009). The 3Ms of central spindle assembly: microtubules, motors and MAPs. Nat Rev Mol Cell Biol 10, 9–20.

Goshima G, Wollman R, Stuurman N, Scholey JM, Vale RD (2005). Length control of the metaphase spindle. Curr Biol 15, 1979–1988.

Gupta ML, Jr., Carvalho P, Roof DM, Pellman D (2006). Plus end-specific depolymerase activity of Kip3, a kinesin-8 protein, explains its role in positioning the yeast mitotic spindle. Nat Cell Biol 8, 913–923.

Hildebrandt ER, Hoyt MA (2001). Cell cycle-dependent degradation of the *Saccharomyces cerevisiae* spindle motor Cin8p requires APC(Cdh1) and a bipartite destruction sequence. Mol Biol Cell 12, 3402–3416.

Hoyt MA, He L, Loo KK, Saunders WS (1992). Two *Saccharomyces cerevisiae* kinesin-related gene products required for mitotic spindle assembly. J Cell Biol 118, 109–120.

Hoyt MA, He L, Totis L, Saunders WS (1993). Loss of function of *Saccharomyces cerevisiae* kinesin-related *CIN8* and *KIP1* is suppressed by *KAR3* motor domain mutations. Genetics 135, 35–44.

Hwang LH, Murray AW (1997). A novel yeast screen for mitotic arrest mutants identifies DOC1, a new gene involved in cyclin proteolysis. Mol Biol Cell 8, 1877–1887.

Juang YL, Huang J, Peters JM, McLaughlin ME, Tai CY, Pellman D (1997). APC-mediated proteolysis of Ase1 and the morphogenesis of the mitotic spindle. Science 275, 1311–1314.

Kawamura M, Maruyama K (1970). Electron microscopic particle length of F-actin polymerized in vitro. J Biochem 67, 437–457.

Khmelinskii A, Lawrence C, Roostalu J, Schiebel E (2007). Cdc14-regulated midzone assembly controls anaphase B. J Cell Biol 177, 981–993.

Kotwaliwale CV, Frei SB, Stern BM, Biggins S (2007). A pathway containing the Ipl1/aurora protein kinase and the spindle midzone protein Ase1 regulates yeast spindle assembly. Dev Cell 13, 433–445.

Lacefield S, Magendantz M, Solomon F (2006). Consequences of defective tubulin folding on heterodimer levels, mitosis and spindle morphology in *Saccharomyces cerevisiae*. Genetics 173, 635–646.

Lundin VF, Srayko M, Hyman AA, Leroux MR (2008). Efficient chaperone-mediated tubulin biogenesis is essential for cell division and cell migration in *C. elegans*. Dev Biol 313, 320–334.

McNally FJ (1996). Modulation of microtubule dynamics during the cell cycle. Curr Opin Cell Biol 8, 23–29.

Moore SA (1987). Alpha-factor inhibition of the rate of cell passage through the "start" step of cell division in Saccharomyces cerevisiae yeast: estimation of the division delay per alpha-factor.receptor complex. Exp Cell Res 171, 411–425.

Murphy DB, Gray RO, Grasser WA, Pollard TD (1988). Direct demonstration of actin filament annealing in vitro. J Cell Biol 106, 1947–1954.

Nakajima Y, Cormier A, Tyers RG, Pigula A, Peng Y, Drubin DG, Barnes G (2011). Ipl1/Aurora-dependent phosphorylation of Sli15/INCENP regulates CPC-spindle interaction to ensure proper microtubule dynamics. J Cell Biol 194, 137–153.

Okreglak V, Drubin DG (2010). Loss of Aip1 reveals a role in maintaining the actin monomer pool and an in vivo oligomer assembly pathway. J Cell Biol 188, 769–777.

Roof DM, Meluh PB, Rose MD (1992). Kinesin-related proteins required for assembly of the mitotic spindle. J Cell Biol 118, 95–108.

Severin F, Habermann B, Huffaker T, Hyman T (2001). Stu2 promotes mitotic spindle elongation in anaphase. J Cell Biol 153, 435–442.

Simon JR, Salmon ED (1990). The structure of microtubule ends during the elongation and shortening phases of dynamic instability examined by negative-stain electron microscopy. J Cell Sci 96, 571–582.

Sprague GF (1991). Assay of yeast mating reaction. Methods Enzymol 194, 77–93.

Srayko M, Kaya A, Stamford J, Hyman AA (2005). Identification and characterization of factors required for microtubule growth and nucleation in the early *C. elegans* embryo. Dev Cell 9, 223–236.

Straight AF, Belmont AS, Robinett CC, Murray AW (1996). GFP tagging of budding yeast chromosomes reveals that protein-protein interactions can mediate sister chromatid cohesion. Curr Biol 6, 1599–1608.

Straight AF, Sedat JW, Murray AW (1998). Time-lapse microscopy reveals unique roles for kinesins during anaphase in budding yeast. J Cell Biol 143, 687–694.

Varga V, Helenius J, Tanaka K, Hyman AA, Tanaka TU, Howard J (2006). Yeast kinesin-8 depolymerizes microtubules in a length-dependent manner. Nat Cell Biol 8, 957–962.

Walczak CE, Heald R (2008). Mechanisms of mitotic spindle assembly and function. Int Rev Cytol 265, 111–158.

Winey M, O'Toole ET (2001). The spindle cycle in budding yeast. Nat Cell Biol 3, E23–E27.

Woodbury EL, Morgan DO (2007). Cdk and APC activities limit the spindle-stabilizing function of Fin1 to anaphase. Nat Cell Biol 9, 106–112.

Woodruff JB, Drubin DG, Barnes G (2010). Mitotic spindle disassembly occurs via distinct subprocesses driven by the anaphase-promoting complex, Aurora B kinase, kinesin-8. J Cell Biol 191, 795–808.

Zimniak T, Stengl K, Mechtler K, Westermann S (2009). Phosphoregulation of the budding yeast EB1 homologue Bim1p by Aurora/Ipl1p. J Cell Biol 186, 379–391.

Supplemental Material

SUPPLEMENTAL FIGURES

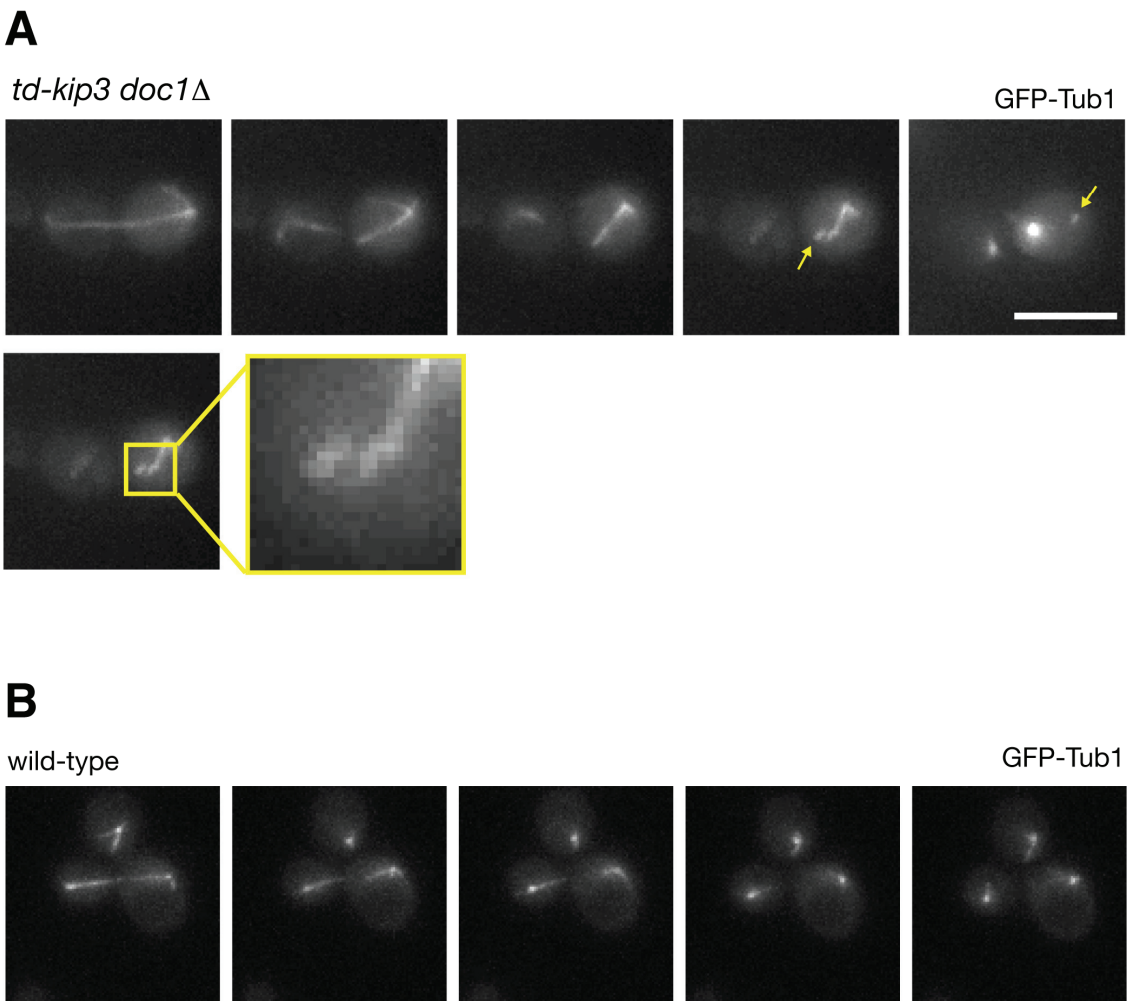

Figure S1. Spindle remnants appear in *td-kip3 doc1Δ* daughter cells following a round of defective spindle disassembly. (A) Time-lapse fluorescent images of *td-kip3 doc1Δ* cells expressing GFP-Tub1 incubated at 37° C. A spindle remnant is indicated with a yellow arrow. The area outlined by the yellow box was magnified 4-fold to illustrate the spindle remnant as it separated from the disassembling spindle. (B) Time-lapse epifluorescence images of wild-type cells expressing GFP-Tub1 incubated at 37° C. No spindle remnants were seen in either daughter cell following spindle disassembly. Scale bar, 5 μm.

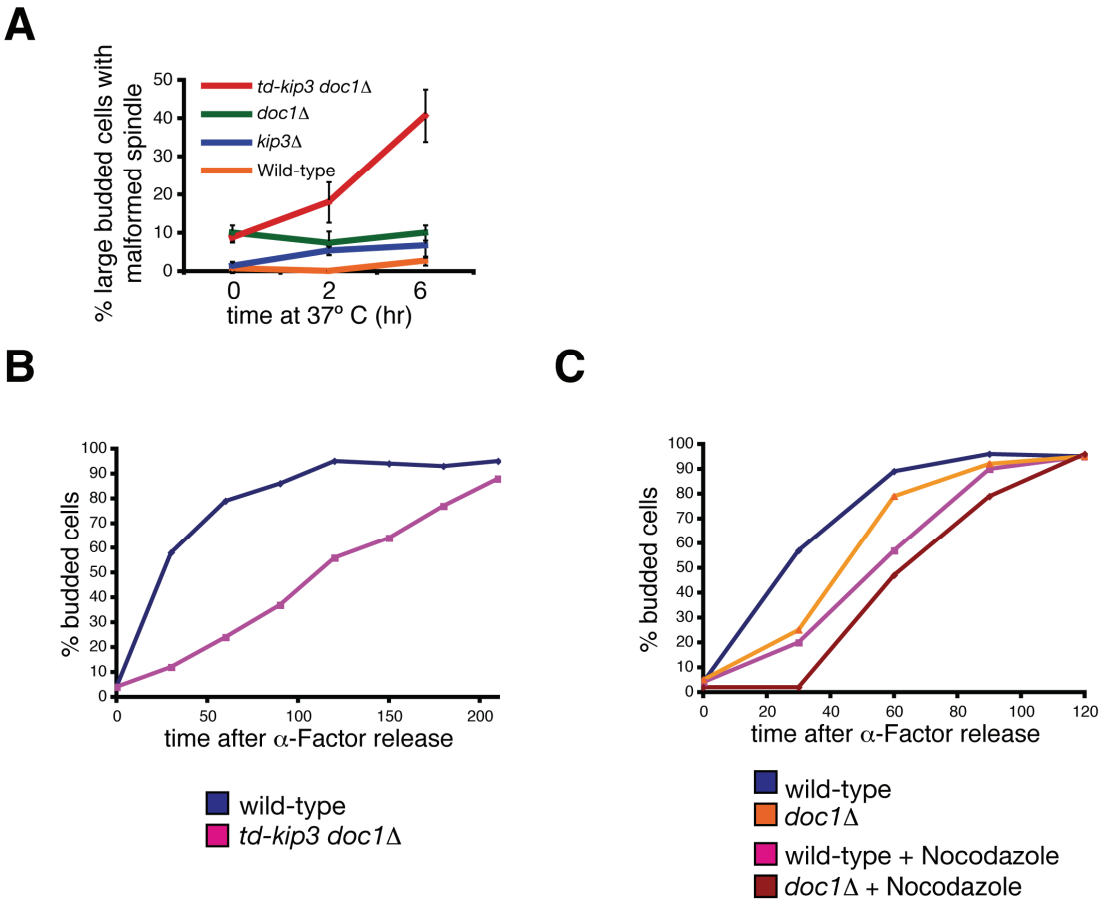

Figure S2. Synergy of the *td-kip3* and *doc1Δ* alleles and budding assays. (A) The frequency of malformed spindles seen in various mutants as a function of time incubated at 37° C. Combining the *td-kip3* and *doc1Δ* mutations had a synergistic effect on spindle assembly (n = 3 experiments each analyzing 50 cells). Incubation at 37° C did not noticeably affect the frequency of malformed spindles seen in wild-type, *kip3Δ*, or *doc1Δ* cells. (B) and (C) The indicated strains were arrested in G1 and then released. The percentage of budded cells was then measured. Cells were incubated at 37° C for the duration of the experiment. Nocodazole or DMSO was added when cells were released from the G1 arrest.

A Diploid Mating Assay

	total colonies	mating colonies	%
Wild-type	4872	2	0.08
*td-kip3 doc1*Δ	2940	1	0.07

B Chromosome III segregation

	sample number (n)	# cells with no GFP-labeled Chr III	%
Wild-type	300	2	0.67
*td-kip3 doc1*Δ	400	4	1

C Mtw1-RFP segregation

	sample number (n)	# cells with no MTW1-RFP	%
Wild-type	100	1	1
*td-kip3 doc1*Δ	100	2	2

Figure S3. Chromosome missegregation rates in wild-type and *td-kip3 doc1Δ* cells. (A) Dipoloid cells were plated on either YPD or minimal medium containing a wild-type *MATa* tester strain. Diploid cells that lose chromosome III bearing the *MATa* gene gain the ability to mate with the tester strain and then grow on the minimal medium. This experiment was performed at 25° C. (B) Chromosome segregation was visualized in cells expressing a LacI-GFP fusion that binds to a tandem array of LacO sequences located on chromosome III. This experiment was performed at 25° C. (C) Cells were synchronized in pre-anaphase with hydroxyurea at 25° C, then released into αF-containing medium at 37° C. Chromosome segregation was monitored throughout anaphase by visualizing the kinetochore marker Mtw1-RFP. Shown are G1 cells. 98% of *td-kip3 doc1Δ* cells had partitioned Mtw1-RFP fluorescence equally without evidence of lagging kinetochores (n = 100).

37° C	sample number (n)	Avg. metaphase aMT length (μm)	P-value
Wild-type	28	2.59 ± 1.1	N.A.
*td-kip3 doc1*Δ	29	1.46 ± 0.8	<0.001

Figure S4. aMT lengths in wild-type and *td-kip3 doc1Δ* cells. GFP-Tub1-expressing cells were synchronized as in Figure 3A and imaged after a 3.5 hr incubation in hydroxurea.

Supplemental Table S1. Yeast Strains.

Strain name	Mating type	genotype	source
JBY 39	*MATa*	*GFP-TUB1::URA3 ADE2*	Woodruff et al., 2010
JBY 401	*MATa*	*ASE1-GFP::TRP1 td-HA-KIP3::URA3 doc1Δ::KanMX6 SPC42-eqFP::NatMX ADE2*	this study
JBY 394	*MATα*	*CIN8-4GFP::KanMX6 td-HA-KIP3::URA3 doc1Δ::KanMX6 SPC42-eqFP::NatMX ADE2*	this study
JBY 210	*MATα*	*td-HA-kip3::URA3 doc1Δ::KanMX6 ADE2*	this study
JBY 398	*MATa*	*td-HA-KIP3::URA3 doc1Δ::KanMX6 MTW1-RFP::HIS3 ADE2*	this study
JBY 399	*MATA*	*pac10(KO)::HIS3 plp1(KO)::hisG yap4(KO)::KanMX6 ADE2 GFP-TUB1::URA3*	this study; Lacefield et al., 2006
JBY 391	*MATa*	*td-HA-kip3::URA3 doc1Δ::KanMX GFP-TUB1::URA3 pGAL::TUB1::TUB2::LEU2 ADE2*	this study; Burke et al., 1989
JBY 380	*MATa*	*td-HA-KIP3::URA3 doc1Δ::KanMX6 SPC42-eqFP::NatMX GFP-TUB1::URA3 ADE2*	this study
JBY 377	*MATa*	*SPC42-eqFP::NatMX GFP-TUB1::URA3 ADE2*	this study; Khmelinskii et al., 2007
JBY 209	*MATa*	*td-HA-kip3::URA3 doc1Δ::KanMX GFP-TUB1::URA3 ADE2*	this study
JBY 150	*MATa*	*kip3Δ::KanMX6 GFP-TUB1::URA3 ADE2*	Woodruff et al., 2010
JBY 386	*MATα*	*td-HA-kip3::URA3 GFP-TUB1::URA3 pGAL::HA-UBR1::HIS3 ADE2*	this study
JBY 156	*MATa*	*doc1Δ::KanMX GFP-TUB1::URA3 ADE2*	Woodruff et al., 2010
JBY 402	*MATa/α*	*GFP-TUB1::URA3/ura3-52 ADE2*	this study
JBY 405	*MATa/α*	*td-HA-kip3::URA3/td-HA-kip3::URA3 doc1Δ::KanMX/ doc1Δ::KanMX GFP-TUB1::URA3/ura3-52 ADE2*	this study
JBY 403	*MATα*	*td-HA-KIP3::URA3 doc1Δ::KanMX6 HIS3::pCu-LacI-GFP leu2-3,112::lacO::LEU2 ADE2*	this study
DDY 4270	*MATa*	*td-HA-KIP3::URA3 doc1Δ::KanMX6 PDS1-18MYC::LEU2*	this study
DDY 4274	*MATa*	*PDS1-18MYC::LEU2 ADE2*	this study
JBY 16	*MATa*	*HIS3::pCu-LacI-GFP leu2-3,112::lacO::LEU2 ADE2*	Woodruff et al., 2009